Journal of Materials Chemistry B

Accepted Manuscript

ROYAL SOCIETY OF CHEMISTRY

www.rsc.org/materialsB

Researching the Dose ratio in a Controlled Release Multiple-drug Delivery System: Using Combination Therapy with Porous Microparticles for the Treatment of *Helicobacter Pylori* Infection

Shilei Hao, Bochu Wang *, Yazhou Wang

Key Laboratory of Biorheological Science and Technology, Ministry of Education, College of Bioengineering, Chongqing University, Chongqing 400030, China

E-mail address: wangbc2000@126.com (B. Wang)

Tel. /Fax: +86-23-6511-2840

Abstract

Combination therapy can improve therapeutic efficacy or reduce side effects due to the synergistic effects between drugs, and the dose ratio, which is a key factor for combination therapy in the clinic, however, had not been considered in previous studies. Therefore, triple-drug-loaded porous microparticles (containing amoxicillin sodium, metronidazole, and omeprazole) were prepared by emulsion electrospray according to an experiential regimen for the combination therapy of *Helicobacter pylori* (*H. pylori*) infection, and the feeding mass ratios of the drugs were optimized to ensure that the mass ratios of released drugs are in accordance with the dose ratios of three drugs in the recommended regimen. In addition, the particle sizes were less than 10 μm, and *in vivo* gamma scintigraphy study demonstrated that the ^{131}I-labeled porous microparticles were retained in the stomach for more than 8 h. Furthermore, the triple-drug-loaded porous microparticles exhibited a stronger effect on *H. pylori* eradication compared to the free drugs. The results indicate that adjustment of the

feeding amounts of drugs is an effective approach for the control of the released amounts of drugs from the diffusion-dependent multiple-drug delivery system. Moreover, the prepared triple-drug-loaded porous microparticles are more suitable for the treatment of clinical *H. pylori* infection.

KEYWORDS: Combination therapy; Multiple-drug delivery; Dose ratio; *Helicobacter pylori*; Porous microparticles

Introduction

The simultaneous administration of two or more drugs is necessary and useful for the clinical therapy of various diseases and can provide a more effective treatment or reduce side effects [1]. In the past several years, many researchers have made considerable efforts to develop multiple-drug delivery systems for combined treatment with sequential chemotherapy [2-4]. This strategy can also be used in tissue regeneration and engineering [5-7] to mitigate the adverse effects induced by some drugs [1, 8, 9] and to fight bacterial infection [10].

In these systems, multiple drugs are entrapped into a single system, and the individual drugs would show different release profiles due to its different hydrophilicities, molecular weights, solubilities, and the incorporated locations in the system [11, 12]. Therefore, the simultaneous and programmable drug release can be controlled in multiple-drug delivery systems [8, 12-15]. However, few studies have focused on the dose ratio of drugs in the design of multiple-drug delivery systems, which are critical to ensure a therapeutic effect and patient safety. To ensure that the dose ratio of the combination therapy is equivalent to the therapeutic dose normally

given in the clinic, the amount of drugs released from the multiple-drug delivery systems should be controlled. The synergistic effects of drugs could be activated if the mass ratio of the released drugs is in accordance with the clinical dose ratio at each time point in the combination therapy.

The aim of the present study was to fabricate novel gastroretentive porous Eudragit® RS (ERS) microparticles loading with multiple drugs for the combination therapy of *Helicobacter pylori* (*H. pylori*) infection. In order to make mass ratio of released drugs equal the dose ratio of three drugs in the therapy regimen, the released amounts of the drugs were then adjusted by changing the feeding amounts of the drugs. Multiple drug therapies containing a proton pump inhibitor and antibiotics are globally recommended regimens for the treatment of *H. pylori* infections in the clinic [16, 17]. However, the first-line treatments have resulted in unsatisfactory eradication rates for *H. pylori* infection (70-85 %) due to the limited gastric residence time of the therapeutic agents [18]. Therefore, some gastroretentive dosage forms loading with single drug have been fabricated to treat *H. pylori* infection in the past decades [19, 20]. In the current study, we have prepared triple-drug-loaded porous ERS microparticles for the combination therapy of *H. pylori* infection and found that these are more suitable for clinical practice [16, 21]. Porous microparticles can remain buoyant in the stomach due to its low bulk density [22], this attribute plays a major role in reducing gastric emptying effects on gastric retention and provide a high drug concentrations in the stomach compared with those obtained using traditional treatments [23].

An experiential triple therapy regimen including 40 mg of omeprazole (OME),

400 mg of metronidazole (MTZ), and 1 g of amoxicillin sodium (AMO) was selected for use in this study [24]. Therefore, the mass ratio of released AMO to MTZ to OME would be 25:10:1. And OME enteric nanoparticles were first synthesized in the present study because OME is unstable in an acidic environment [25]. The physicochemical characteristics of the triple-drug-loaded porous microparticles generated by emulsion electrospray were examined, and single-photon emission computed tomography (SPECT) was employed to investigate the *in vivo* floating behavior of the porous microparticles in rabbits. Furthermore, the *in vitro* and *in vivo* *H. pylori* clearance abilities of the triple-drug-loaded porous microparticles were studied, and histological examination was used to detect tissue inflammation in *H. pylori*-infected mouse models.

Experimental Sections

Materials

Eudragit® RS PO (ERS，MW=32 kDa) and Eudragit® L 100-55 (EL 100-55，MW=320 kDa) were type gifts from Evonik Industries (Essen, Germany). Metronidazole (MTZ) and omeprazole (OME) were kindly gifted by Southwest Pharmaceutics Co., Ltd. (Chongqing, China). Amoxicillin sodium (AMO) was supplied by Tuchukangyuan Pharm and Chem Co., Ltd. (Hubei, China). Dichloromethane was purchased from Chuandong Reagent Factory (Chongqing, China). The human gastric epithelial cell line (GES-1) was supplied by the Institute of Pathology, Southwest Hospital (Chongqing, China). MTT was supplied by Amresco (Solon, USA). Iodine-131 (^{131}I) was supplied by the Department of Nuclear Medicine, Chongqing Cancer Hospital

(Chongqing, China). *H. pylori* strain 26695 (ATCC 700392) was supplied by the Department of Clinical Microbiology and Clinical Immunology, Third Military Medical University (Chongqing, China). All of the other materials and reagents used in the present study were of analytical grade.

Preparation of dual-drug-loaded porous microparticles

It is not easy to obtain ideal drug release profiles by simultaneous changing the feeding mass ratios of three drugs, and the simultaneous quantitative analysis of OME, MTZ, and AMO using an UV spectrophotometer or HPLC is also quite difficult. Therefore, we first created two different dual-drug-loaded porous microparticles: MTZ/OME-loaded porous microparticles and MTZ/AMO-loaded porous microparticles. The drug loading ratio of MTZ to OME and AMO to MTZ in dual-drug-loaded porous microparticles were adjusted by changing the feeding mass ratio of drugs, and then the optimal feeding mass ratios of MTZ to OME and MTZ to AMO would obtained when mass ratio of release AMO to MTZ and MTZ to OME were close to 2.5:1 and 10:1, respectively. The final decided feeding mass ratio of three drugs would be used to prepare the triple-drug-loaded porous microparticles. The schematic illustration of formation of triple-drug-loaded porous microparticles was shown in Fig. 1.

Preparation of blank porous microparticles

The blank porous microparticles were prepared by emulsion electrospray. The water-in-oil (W/O) emulsions were prepared as the spray solution: 100 mg of ERS was dissolved in dichloromethane (10 mL) as the oil phase, and the W/O emulsion

was synthesized by the addition of 0.5 mL of acetic acid aqueous solution (pH 5.0) to 10 mL of the oil phase with sonication on ice for 30 s at 400 W. The ultrasonication was supplied by an ultrasonic cell disruption system (JY92-II, Scientz, China). The spray solution was supplied by a syringe pump (TJ-3A, Longer, China) that sprayed from the grounded nozzle (inner diameter, 0.88 mm; outer diameter, 1.27 mm). The nozzle was connected to a positive electrode (+10 kV) of a high-voltage power supply (DW-P503-1AC, Dongwen, China). The flow rate of the solution was 900 μL/h, and aluminum foil was placed perpendicular to the nozzle as a collector. The distance between the nozzle and aluminum foil was 100 mm.

Preparation of dual-drug-loaded porous microparticles

The drug-loaded porous microparticles were prepared by the addition of MTZ into the oil phase and the addition of AMO and OME enteric nanoparticles into the water phase. The OME-loaded EL100-55 nanoparticles were first prepared as described in our previous study [25], and the drug loading of EL 100-55 enteric nanoparticles was 43.21 %. The dual-drug-loaded porous microparticles with different drug loading were fabricated as follow: the feeding amount of OME enteric nanoparticles was fixed to 6.0 mg, and different amounts of MTZ ranging from 20 to 35 mg were fed into the MTZ/OME-loaded porous microparticles. Similarly, the feeding amount of MTZ was fixed to 15 mg, and different amounts of AMO ranging from 25 to 40 mg were fed into the MTZ/AMO-loaded porous microparticles.

Drug loading measurements

The loading capacity and entrapment efficiency of the two different dual-drug-loaded

porous microparticles (MTZ/OME and MTZ/AMO) were determined by the following method. The drug-loaded porous microparticles were incubated in dichloromethane to dissolve the microparticles. PBS buffer solution (pH 7.4) was then added to the solution, and the mixed solution was stirred until the dichloromethane was completely volatilized. The contents of MTZ and OME in the solution were detected using a UV spectrophotometer with differential analysis at 340 nm and 300 nm, respectively (Lambda 900, PerkinElmer, USA). Similarly, the concentrations of MTZ and AMO in the solution were also detected by differential spectrophotometry at 340 nm and 230 nm, respectively. The loading capacity and entrapment efficiency were calculated using Eq. (1) and Eq. (2):

$$\text{Loading capacity} = \frac{\text{Weight of drug in microparticles}}{\text{Weight of microparticles}} \times 100\% \qquad (1)$$

$$\text{Entrapment efficiency} = \frac{\text{Loading capacity of microparticles}}{\text{Loading capacity of microparticles in theory}} \times 100\% \qquad (2)$$

In vitro release studies

The aims of the *in vitro* release study were to investigate the release profiles of the drugs from the dual-drug-loaded porous microparticles and to optimize the feeding mass ratio of three drugs. The two different dual-drug-loaded porous microparticles (MTZ/OME and MTZ/AMO) and 3 mL of SGF (pH 1.2) were added to each of two dialysis tubes. The dialysis tubes were then placed in 30 mL of SGF at 37 °C with shaking at 100 rpm for 12 h. At specific time intervals, the medium (1 mL) was removed and replaced with fresh SGF. The concentration of the released drugs in the SGF was determined by UV spectrophotometry. In addition, drug release studies of

the MTZ/OME-loaded porous microparticles were also performed in simulated intestinal fluid (SIF, pH 6.8) because OME would not be released from enteric nanoparticles in an acidic environment.

Optimization of the feeding mass ratio of drugs

The dose ratio of drugs in a combination therapy can be represented as the mass ratio of the released drugs from a controlled release multiple-drug delivery system. The dose ratio of MTZ to OME is 10:1 in the recommended regimen, whereas the dose ratio of MTZ to AMO is 1:2.5. The released amounts of MTZ and OME from the MTZ/OME-loaded porous microparticles in the SIF were measured to optimize the feeding mass ratio of MTZ to OME. Similarly, the released amounts of MTZ and AMO from the MTZ/AMO-loaded porous microparticles in the SGF were also measured to optimize the feeding mass ratio of MTZ to AMO.

Preparation of triple-drug-loaded porous microparticles

The triple-drug-loaded porous microparticles were prepared in a similar manner as the dual-drug-loaded porous microparticles. MTZ was added into the oil phase, and the AMO and OME enteric nanoparticles were added into the water phase. The optimized feeding mass ratios of the three drugs were used to prepare the triple-drug-loaded porous microparticles. The effect of different ERS concentrations (from 1% to 4%) on the characterization of the triple-drug-loaded porous microparticles was investigated in this study.

Characterization of triple-drug-loaded porous microparticles

The viscosities of electrospray solutions with different ERS concentrations ranging

from 1 % to 4 % (containing drugs) were detected using a digital viscometer (NDJ-8S, Hengping, China).

The surface morphology of the triple-drug-loaded porous microparticles with different ERS concentrations was observed by scanning electron microscopy (SEM) and transmission electron microscopy (TEM). A piece of aluminum foil loading with porous microparticles was coated with gold metal under vacuum and then examined by SEM (EVOLS25, Zeiss, Germany). The microparticle suspensions were dropped on copper grids, natively stained with phosphotungstic acid, and dried at room temperature for the TEM observations (Tecnai G2 20, FEI, USA). Furthermore, the morphology of the triple-drug-loaded porous microparticles after incubation in SGF for different times (1, 2, 4, 6, and 8 h) was observed using SEM. The protocol used for the incubation of the porous microparticles in SGF was similar to that used in the drug release studies. At specific time intervals, the porous microparticles in the dialysis tubes were transferred to a piece of aluminum foil, and the resulting porous microparticles were then lyophilized (230, Modulyod, USA) and examined.

The particle size distribution and polydispersity index (PDI) of the triple-drug-loaded porous microparticles were measured using a laser light scattering particle size analyzer (3500S, Microtrac Inc., USA). The zeta potentials of the porous microparticles were analyzed using a Zetasizer (Nano ZS90, Malvern, UK). The samples were diluted to appropriate concentrations with deionized water. In addition, the samples were also diluted with SGF to determine the zeta potential.

The bulk density and tap density of the triple-drug-loaded porous microparticles

with different ERS concentrations (from 1% to 4%) were measured as described previously [26]. The weight of the microparticles filling a 1-mL graduated syringe was recorded to calculate the bulk density. The tap density of the porous microparticles was evaluated by tapping on a hard bench until there was no further change in the volume of the porous microparticles. The resultant volume was recorded to calculate the tap density.

The chemical structure and complex formation of OME, MTZ, AMO, ERS, EL 100-55, OME-loaded EL 100-55 nanoparticles, and triple-drug-loaded porous microparticles were analyzed by FT-IR (5DX/550, Nicolet, USA). The samples used for the FT-IR spectroscopic characterization were prepared by grinding the dry specimens with KBr and pressing them to form disks.

The XRD experiments were conducted using an X-ray diffractometer (6000X, Shimadzu, Japan). OME, MTZ, AMO, ERS, EL 100-55, OME-loaded EL 100-55 nanoparticles, triple-drug-loaded porous microparticles, and a physical mixture of the drugs and polymers were analyzed in at a 2θ ranging from 5 degrees to 45 degrees with a step width of 0.04 degrees and a count time of 2 seconds.

***In vitro* cytotoxicity study**

GES-1 cells were used for the cytotoxicity test. The cells were seeded in 96-well plates at a density of 1×10^4 cells per well. For the concentration-dependent cytotoxicity experiments, the suspensions of triple-drug-loaded porous microparticles were diluted with culture medium to different concentrations. The cells were incubated with the microparticles at concentrations ranging from 25 to 800 mg/L for

24 h. For the time-dependent cytotoxicity experiments, the GES-1 cells were incubated with the drug-loaded porous microparticles at different ERS concentrations ranging from 1 % to 4 % (50 mg/L) and blank microparticles for 12, 24, 36, and 48 h. After the addition of the MTT solution, absorption at 490 nm was measured using a microplate reader (Model 3550, Bio-Rad, USA). The results are expressed as the percentage of reduction in cell growth/viability compared to untreated control wells, and cells that were not incubated with MTT were used as a blank to calibrate the spectrophotometer to zero absorbance.

In vivo evaluation of gastric retention ability of porous microparticles

Radiolabeling of porous microparticles

Iodine-131 (^{131}I) was selected to radiolabel the triple-drug-loaded porous microparticles because its half-life is 8.02 days. An aliquot of ^{131}I solution equivalent to a radioactivity of 5 mci was added to the tube. The labeled porous microparticles were recovered by filtration through a filter paper and dried overnight at room temperature. All of the operations were performed in a fume hood.

Stability of radiolabeled porous microparticles

The stability of the ^{131}I-labeled porous microparticles was tested as follows: the ^{131}I-labeled porous microparticles (5 mg) were first placed into three tubes, and three different standard buffer solutions (pH 1.2, 6.8, and 7.4) were added individually to these three tubes. The tubes were placed in a water bath at 37 °C for 8 h. At predetermined time intervals, 0.2-mL samples were collected using a pipette attached to a 0.45-μm cellulose acetate filter, and the porous microparticles were then

recovered, washed, and dried. The radioactivities of the microparticles, the filtrate, and the filter were determined using an auto gamma counter (CRC-25R, Capintec, USA).

Gamma imaging in rabbits

Three adult male New Zealand white rabbits weighing approximately 2–2.5 kg were used in the study. No rabbits were taking any regular medication or had a history of gastrointestinal disorders. All of the animal experiments were approved by the Animal Ethical and Experimental Committee of the Third Military Medical University. After fasting for 24 h, the rabbits were orally administered the ^{131}I-labeled porous microparticles (30 μci) through a gastric tube with 20 mL of water. The rabbits were not allowed to eat or drink during the imaging period. Scintigrams were recorded using a single-photon emission computed tomography (SPECT) apparatus with variable angle dual-detector units (Symbia T2, Siemens, USA). At predetermined time intervals, the rabbits underwent anterior whole-body static scintigraphy for 2 min.

The *in vivo* biodistribution of ^{131}I-labeled porous microparticles was scanned after the gamma scintigraphy studies using a hybrid scanner comprised of a two-row spiral CT and a SPECT camera (Symbia T2, Siemens, USA). Immediately after the SPECT and CT data were acquired, the raw data were reconstructed into transverse, coronal, and sagittal slices using a Siemens' powerful *syngo*®-software-based *e.soft*™ workstation (Siemens Medical Solutions). The image reconstruction using a high-resolution reconstruction algorithm (B70 kernel) resulted in images with a slice thickness of 3 mm for a 1.5-mm reconstruction increment. During both the SPECT

and the CT scans, the rabbits were lying stably in a supine position. The processed SPECT and CT images were reviewed for adequacy of quality, attenuation correction, registration, and fusion by a nuclear medicine specialist.

Image analysis

A region of interest (ROI, a circle with a diameter of 100 mm) was drawn to determine the ^{131}I radioactivity in the stomach at different time points. The ROI quantification was performed with the *syngo*® MI Acquisition Workplace (Siemens Medical Solutions). The radioactivity in the ROI at 0 h was taken considered the control and designated as 100 %.

***In vitro H. pylori* Growth Inhibition Study**

The standard strain of *H. pylori* 26695 (ATCC 700392) was maintained on brain-heart infusion (BHI) plates containing 10 % rabbit blood and antibiotics under microaerobic conditions (4 % O_2, 11 % CO_2, and 85 % N_2) in a variable atmosphere incubator at 37 °C. After 2 to 3 days of culture, the bacterial colonies were collected and suspended in BHI to a final concentration of 1×10^7 colony forming units (CFU)/mL.

The *in vitro* growth inhibition studies were conducted as follows: the bacterial suspensions (30 mL) and test samples were incubated together for 12 h with shaking at 220 rpm for 12 h. The samples were placed into a dialysis tube (MWCO: 12,000 Da) during the study. To simulate the *in vivo* elimination of drugs, the bacteria were harvested by centrifugation at 5,000 rpm and 4 °C for 5 min after 2 h of incubation. Half of the bacterial suspension was removed and replaced with fresh BHI. At predetermined time intervals, bacterial suspensions (0.5 mL) were collected, and

serial dilutions (50 μL) were plated on BHI plates. After 5 days of cultivation under microaerobic conditions, the viable bacterial count was calculated by counting the number of colonies on the BHI plates. AMO at a concentration of 0.125 μg/mL was used in the inhibition study, and OME nanoparticles and MTZ were also added at the chosen mass ratios.

In vivo* clearance of *H. pylori

Mice and infection

SPF female C57BL/6 mice aged 6-8 weeks were purchased from the Experimental Animal Center of the Third Military Medical University. After an overnight fast, the mice were orally infected with *H. pylori* 26695 through the inoculation of 0.3 mL of broth containing approximately 10^9 CFUs of *H. pylori* per mL into the stomach of each mouse using an oral feeding needle. The mice were administered this dose twice daily for three consecutive days. Four weeks after the initial infection, the infected mice were randomly divided into ten different groups ($n=4$ per group).

Different drug regimens containing triple-drug-loaded porous microparticles and free drugs were used to treat the *H. pylori* infection for three consecutive days. OME enteric nanoparticles were used in the porous microparticles and free drug regimens. The frequency of the triple-drug-loaded porous microparticles was once daily (QD), and the free drugs were administered QD and twice daily (BID). In addition, three regimens with different doses (low, middle, and high) were also studied. The MTZ concentrations for the low, middle, and high dose groups were 5, 15, and 25 mg/kg, respectively. The OME nanoparticles and AMO were also added at determined mass

ratios. Normal saline was orally administered (QD) in the same manner as the control group. One week after the administration of the final dose, the stomachs of the mice were removed and subjected to the following tests.

Histopathological examination of mouse stomachs

Narrow strips of tissue were surgically removed from the greater curvature of the stomach and from the duodenum to the gastric cardia. The gastric samples were fixed in 10 % neutral buffered formalin and embedded in paraffin. Hematoxylin and eosin staining was performed by the Institute of Pathology, Southwest Hospital (Chongqing, China) using a standard histological technique. The gastric tissue was evaluated blindly for the extent, depth, and character of inflammation at the antral-fundic junction.

Determination of H. pylori bacterial counts in the stomach

The stomach was opened along the lesser curvature and dissected into two tissue fragments. The fragments were homogenized in 1 mL of BHI with a tissue homogenizer (Precellys 24, Bertin, France). Tenfold serial dilutions of the homogenate were plated on BHI plates and cultivated under microaerobic conditions. When present, *H. pylori* bacteria were confirmed by their characteristic colony morphology, Gram staining, and catalase, oxidase, and urease activities. After five days of culture, the colonies were counted, and the number of CFUs per gram of stomach was calculated.

Statistical analysis

All of the measurements were performed at least in triplicate, and the data are

presented as the means ± standard deviation (SD). For selected evaluation tests, the means of all tested formulations were compared with each other through one-way ANOVA with one-tailed Student's t-test. The statistical analyses were performed with the SPSS v 17.0 software. The statistical significance level (*P*) was set to $p< 0.05$.

Results

Preparation of triple-drug-loaded porous microparticles

Preparation of dual-drug-loaded porous microparticles

Table 1 shows the effect of different feeding amounts of MTZ on the characterization of the MTZ/OME-loaded porous microparticles (1% ERS). The feeding amount of the OME enteric nanoparticles was selected to be 6.0 mg. The entrapment efficiencies of MTZ and OME were approximately 100 %, and the loading capacity of MTZ increased linearly from 15.92 % to 24.59 % with an increase in the MTZ feeding amount from 20 to 35 mg. The loading capacity of OME decreased linearly from 2.06 % to 1.86 %.

Table 2 shows the effect of different feeding amounts of AMO on the characterization of the MTZ/AMO-loaded porous microparticles, and the feeding amount of MTZ was selected to be 15 mg. The loading capacity of MTZ decreased from 10.72 % to 9.59 %, and the loading capacity of AMO increased from 17.79 % to 25.77 % with an increase in the feeding amount of AMO. An ultrahigh entrapment efficiency of three drugs were also noted in the present study, which indicated that there were no competition relationship among the drugs.

In vitro release studies

The release profiles of MTZ and OME from the MTZ/OME-loaded porous microparticles with different feeding amounts of MTZ (15, 20, 25, and 35 mg) were investigated in SGF (pH 1.2) and SIF (pH 6.8). The feeding amount of OME enteric nanoparticles was 6.0 mg. Fig. 2A-a shows the release profile of MTZ from the MTZ/OME-loaded porous microparticles in SGF. MTZ displayed sustained release in SGF, and the release rate of MTZ was faster from microparticles with a higher feeding amount of MTZ. In addition, OME demonstrated a pH-sensitive release *in vitro*; approximately 10 % of the OME was released from the MTZ/OME-loaded microparticles into the SGF (Fig. 2A-b). Similarly, a sustained release of MTZ from the MTZ/OME-loaded microparticles in SIF was also observed (Fig. 2A-c), and this behavior was due to the pH-independent time-controlled release of ERS. The OME-loaded enteric nanoparticles displayed a faster drug release profile in SIF, but sustained release profiles were also observed when OME was released from the porous microparticles (Fig. 2A-d). This release profile most likely resulted from the strong sustained release effect of ERS.

To optimize the feeding mass ratio of MTZ to OME, the release amounts of MTZ and OME from the MTZ/OME-loaded porous microparticles with different feeding amounts of MTZ in SIF were measured (Fig. 2B). The dosage ratio of MTZ to OME in the recommend regimens is 10:1, and the released amounts of MTZ were less than 10-fold higher than the released amounts of OME at each point when the feeding amounts of MTZ were 20 mg (Fig. 2B-a) and 25 mg (Fig. 2B-b). The mass ratio of MTZ to OME in the release medium was higher when a higher amount of

MTZ was fed into the MTZ/OME-loaded porous microparticles, and the mass ratio of MTZ to OME in the release medium was approximately 10:1 at each time point when the feeding amount of MTZ was increased to 30 mg (Fig. 2B-c). Furthermore, the mass ratio of MTZ to OME far exceeded 10 as the feeding amount of MTZ increased to 35 mg (Fig. 2B-d); thus, the final feeding mass ratio of MTZ to OME nanoparticles was selected to be 5:1.

MTZ/AMO-loaded porous microparticles were also prepared to investigate the drug release profiles and optimize the mass ratio of MTZ to AMO. Fig. 3A-a and Fig. 3A-b show the release profiles of AMO and MTZ from MTZ/AMO-loaded porous microparticles with different feeding amounts of AMO (from 25 to 40 mg) in SGF, respectively. The feeding amount of MTZ was 15 mg. Sustained release profiles of AMO and MTZ were observed, and the release rate of AMO from the porous microparticles increased slightly with an increase in the feeding amount of AMO, which may be a result of the increased drug loading.

The released amounts of MTZ and AMO from MTZ/AMO-loaded porous microparticles with different feeding amounts of AMO were also measured to optimize the feeding ratio of AMO to MTZ (Fig. 3B). The dose ratio of AMO to MTZ is 2.5:1 in the recommended regimen, and the optimized feeding ratio of AMO to MTZ would be obtained if the released amount of AMO is equal to 2.5-fold higher than the released amount of MTZ at each time point. Fig. 3B-a and Fig. 3B-b show the cumulative released amounts of MTZ and AMO from MTZ/AMO-loaded porous microparticles with feeding amounts of AMO of 25 and 30 mg, respectively, and the

released amounts of AMO were lower than 2.5-fold higher than the released amounts of MTZ. In addition, the released amounts of AMO did not meet the demand until the feeding amount of AMO increased to 35 mg (Fig. 3B-c), and the mass ratio of AMO to MTZ exceeded 2.5 as the feeding amount of AMO increased to 40 mg (Fig. 3B-d). Thus, the final feeding mass ratio of AMO to MTZ was 7:3, and the optimized feeding amounts of AMO, MTZ and OME in the preparation of the triple-drug-loaded porous microparticles were 35, 15, and 3 mg, respectively. The results of drug release studies indicate that adjustment of the feeding amounts of drugs is an effective approach for the control of the released amounts of drugs from the diffusion-dependent multiple-drug delivery system.

Preparation of triple-drug-loaded porous microparticles

The triple-drug-loaded porous microparticles were prepared according to the optimized feeding mass ratios of the drugs, and the effects of different polymer concentrations on the characterizations of the triple-drug-loaded porous microparticles were studied (Table 3). The mean particle size increased from 2.83 to 9.30 μm as the polymer concentration increased from 1 % to 4 %, which may be due to the increased solution viscosity. The viscosity of the spray solutions increased from 9.13 to 14.20 mPa·s with an increase in the ERS concentration. An increase in the viscosity is thought to increase the resistance of the solution to be separated into droplets, leading to an increased particles size. The ERS porous microparticles also displayed positive zeta potential values in water and SGF, and the zeta potential in SGF, which ranged from +41.09 to +50.34 mV, was higher than that found in water (from +13.39 to

+21.92 mV). High zeta potential would facilitate the stability of microparticle suspension and prevent the nanoparticles from aggregation [25]. Furthermore, low tap density values (less than 0.110 g/cm^3) were detected, and these were smaller than the density of the gastric content (≈1.004 g/cm^3) [27], which demonstrated that the prepared porous microparticles may have a strong gastric retention ability *in vivo*.

Characterization of triple-drug-loaded porous microparticles

Morphology

Fig. 4A shows the SEM and TEM images of ERS porous microparticles with different ERS concentrations (from 1 % to 4 %). The pore size of the microparticles decreased as the polymer concentration increased, which also led to an increase in the particle size. Increasing polymer concentration would increase the resistance of the solution to be separated into droplets and then result in a large size of porous microparticles. In addition, some cavities were observed on the surface, an effect that was likely due to the inhomogeneous distribution of polymer molecules on the surface during the drying process. Furthermore, an obvious porous structure can be observed in the TEM images.

Furthermore, the morphology of the triple-drug-loaded porous microparticles (1 % ERS) after incubation in SGF for different times was also studied (Fig. 4B). After a 2-h incubation period, the porous microparticles became swollen, and the surface pores disappeared. However, the shapes of the porous microparticles were also irregular with some caving on the surface (Red arrows). In addition, an increasing number of ERS microparticles demonstrated fusion with extended

incubation times (Green arrows). However, there was no big difference from SEM images of triple-drug-loaded porous microparticles after incubation in SGF for different times, indicated that porous microparticles could remain stable in the SGF, and then provided sustained release of drugs in the stomach.

FTIR study

Our previous studies included FTIR studies of OME, EL100-55, and OME-loaded EL 100-55 nanoparticles [25]. Our results showed that no new bands are observed in the IR spectra of the OME-loaded EL100-55 nanoparticles with the exception of the characteristic bands of OME and EL 100-55 (Fig. 5A). A number of bands characteristic of ERS, including 2955 cm^{-1} (CH_X vibrations), 1732 cm^{-1} (C=O ester vibration), and 1151 cm^{-1} (-COOR stretching), were observed in the spectra of the triple-drug-loaded porous microparticles, but the characteristic bands of OME and MTZ were not found. This result may be due to the low OME and MTZ loading in the triple-drug-loaded porous microparticles. However, the characteristic band of AMO at 1610 cm^{-1} (C=C stretching) was found in the spectra of the triple-drug-loaded porous microparticles because of the high drug loading, and no new bands were observed, indicating that no chemical reaction occurred between the drugs and the polymer.

XRD study

XRD studies of OME, EL 100-55, and OME-loaded EL 100-55 nanoparticles were also included in our previous research efforts, and the results demonstrated that OME becomes entrapped in the enteric nanoparticles (Fig. 5B) [25]. Similar results were observed in the diffractogram of the triple-drug-loaded porous microparticles. The

specific peaks of OME (at 12.3° and 17.2°), MTZ (at 12.3°, 25.4°, 29.3° and 33.4°), and AMO (12.3°, 15.1°, 18° and 19.3°) were observed in the diffractogram of the triple-drug-loaded porous microparticles. However, the intensities of the diffraction peaks in the diffractogram of the microparticles were lower compared with those found in the physical mixture. This difference may be because the characteristic peaks of the drugs were partly overlapped with the noise of the coated polymer itself [8].

***In vitro* cytotoxicity study**

The MTT assay was used to evaluate the cytotoxicity of the triple-drug-loaded porous microparticles. A decrease in the cell viability was observed with an increase in the concentration of the triple-drug-loaded porous microparticles (Fig. 6A). And a significant decrease in cell viability was not observed until the concentration of the triple-drug-loaded microparticles increased to 100 mg/L. The cytotoxicities of the triple-drug-loaded porous microparticles with different ERS concentrations ranging from 1 % to 4 % and the blank microparticles after incubation with cells for 12, 24, 36, and 48 h were investigated in the subsequent studies (Fig. 6B). The cell viability decreased as the polymer concentration decreased, an effect that may be explained by the fact that a low ERS concentration would increase the mass ratio of the drug to the polymer and thereby enhance the drug loading. In addition, the cytotoxicity of the porous microparticles also increased with an increase in the incubation time. However, the cytotoxicity of the blank porous microparticles was not significantly different from that of the control group, regardless of the incubation period, indicating that the main cytotoxicity of the triple-drug-loaded porous microparticles results from the

toxicity of the drugs. The minimum cell viability obtained in this study was higher than 70 % after treatment with the triple-drug-loaded porous microparticles, illustrating that the *in vitro* cytotoxicity of the porous microparticles is low [28].

***In vivo* evaluation of gastric retention ability of porous microparticles**

The stabilities of the ^{131}I-labeled porous microparticles in standard buffer solutions with pH values of 1.2, 6.8, and 7.4 were first tested to confirm that the ^{131}I remained bound to the microparticles for the duration of the study. The activity released from the ^{131}I-labeled porous microparticles was approximately 3.31 ± 0.21 % in pH 1.2, 3.97 ± 0.33 in pH 6.8, and 4.00 ± 0.19 % in pH 7.4 after 8 h. In addition, the nuclide stability is also important for the quantitative determination of the radioactivity of ^{131}I-labeled porous microparticles in the ROI. A long half-life nuclide ^{131}I (8.02 days) was used to label the porous microparticles in our study, and only approximately 2 % of the ^{131}I had decayed after 8 h.

Fig. 7 shows the gamma scintigraphic images of the fasted rabbit 0.5 to 8 h after the oral administration of ^{131}I-labeled triple-drug-loaded porous microparticles. The outline of the rabbit was drawn manually based on the actual rabbit to enable the visual observation of the hotspot movements. An intense hotspot could be observed in the stomach, indicating that the porous microparticles remained in the stomach. The porous microparticles began to be moved to the intestine after 2 h due to the peristalsis of the stomach, and a hotspot also appeared in the thyroid gland of the rabbit as a result of free ^{131}I. However, more than half of the porous microparticles were retained in the stomach of rabbit after 8 h, which demonstrates that the porous

microparticles have good gastro-retentive ability.

An *in vivo* biodistribution study is a necessary supplement to the gamma scintigraphy study and may provide a better anatomical localization of hotspots in hybrid imaging using SPECT/CT techniques. The SPECT and CT images of the rabbit were recorded 8 h after the oral administration of ^{131}I-labeled porous microparticles, and the planar SPECT, CT and SPECT/CT fused images were reconstructed into transverse (Fig. 8A), sagittal (Fig. 8B), and coronal slices (Fig. 8C) with 3.0 mm slice thickness to identify the hotspots. We have supplied 3 transverse slices, 4 sagittal slices and 4 coronal slices. The SPECT/CT fused images demonstrated that the hotspot observed in the gamma scintigraphy is due to the I^{131}-labeled porous microparticles in the stomach. ROI (a circle with a diameter of 100 mm) was also drawn manually around the stomach to measure the radioactive counts in the stomach. Fig. 8D displays the radioactive counts of ^{131}I-labeled porous microparticles in the ROI every two minutes for a period of 8 h. The radioactive counts in the ROI decreased with time during the gamma scintigraphy studies, and approximately 48 % of the radioactive counts remained in the ROI at 8 h.

***In vitro H. pylori* growth inhibition study**

The *in vitro H. pylori* growth inhibition effects of the triple-drug-loaded porous microparticles, free drugs, and blank porous microparticles were investigated, and the results are shown in Fig. 9A. The triple-drug-loaded porous microparticles displayed a sustained inhibition effect compared with the free drugs. However, the free drugs exhibited a stronger inhibition effect than the triple-drug-loaded porous microparticles

at the early time points (within 6 h), and the CFU number increased steadily after 1 h of treatment with the free drugs. The results indicate that the triple-drug-loaded porous microparticles can provide a sustained inhibition effect on *H. pylori* growth compared with the free drugs, although the free drugs display a stronger inhibition effect at the early time points. Furthermore, the blank porous microparticles appeared to have no inhibitory effect on *H. pylori* growth *in vitro*, and the growth curve was similar to that of the control group.

In vivo* clearance of *H. pylori

The *in vivo* clearance of *H. pylori* infection after treatment with the triple-drug-loaded porous microparticles and free drugs was studied. Each dose of the triple-drug-loaded porous microparticles and the corresponding free drugs was divided into three dosage groups: low dose (Fig. 9B), middle dose (Fig. 9C), and high dose (Fig. 9D). The free drug groups were divided into two groups (QD and BID) according to the different administration frequencies. The mean bacterial counts of *H. pylori* decreased with an increase in the dose, and the porous microparticles displayed a stronger *H. pylori* clearance effect than the pure drugs with the same administration frequency (QD). However, a complete clearance of *H pylori* was observed after the administration of a low dose of porous microparticles and the middle doses of the free drugs with BID dosing. These results indicate that the porous microparticles can eradicate *H. pylori* completely with a lower dose of drugs and administration frequency compared with the free drugs.

In addition, the pathological changes in the stomachs of infected mice before and

after the triple therapy were examined. The gastric tissue biopsies were stained with hematoxylin and eosin for histological examination (Fig. 10). Inflammatory cell infiltration by neutrophils and lymphocytes (blue arrows), superficial damage and atrophic changes (black arrows) in the gastric mucosa, inflammatory cell infiltration from the lamina propria mucosa to the submucosa at sites of mucosal damage, and necrosis of the epithelium (red arrows) were observed in the histological images of the stomachs of infected mice. The inflammatory cells decreased and the pathological damage to the surface epithelium was alleviated after the triple therapy. However, slight pathological damage to the surface epithelium could be observed even after treatment with the high doses of the free drugs and porous microparticles, an effect that may be explained by the fact that the healing process for superficial damage is slow compared with the killing of bacteria. Furthermore, the gastric mucosal damage observed in the infected mice after treatment with free drugs with QD dosing was more severe than that observed in the mice treated with the free drugs with BID dosing and porous microparticles, indicating that the porous microparticles are more helpful for the healing of superficial damage than the free drugs under the same doses and administration frequency.

Discussions

An increasing number of multiple-drug delivery systems have been developed in recent years, and these are used for combination therapies for some diseases. However, the dose ratio of drugs is an inevitable problem for the clinical application of multiple-drug delivery systems. The dose ratio of drugs in a clinical trial of

combination therapy may be represented as the mass ratio of the released drugs by the multiple-drug delivery systems; thus, the combination therapy can be successful through the control of the mass ratios of the released drugs at each time point. The drug release rate can be influenced by various factors, including hydrophility, molecular weight, solubility, and the location of drugs in the system. However, the recommend regimens in the combination therapies used for specific diseases and the properties of drugs are usually unchangeable, and it is difficult to design a specific multiple-drug delivery system for the combination of different drugs. The release of drugs from polymeric systems often follows diffusion; thus, the adjustment of drug loading would be an effective approach for the control of the amount of drugs released by most diffusion-dependent drug delivery systems.

In the present study, we prepared triple-drug-loaded porous microparticles by emulsion electrospray for the treatment of *H. pylori* infection. An experimental triple therapy regimen including 40 mg of OME, 400 mg of MTZ, and 1 g of AMO was selected. Two different dual-drug-loaded porous microparticles (MTZ/OME and MTZ/AMO) were first prepared with different drug loadings, and the optimal feeding mass ratios of MTZ to OME and MTZ to AMO were obtained by measuring the released amounts of drugs from the corresponding dual-drug-loaded porous microparticles. Based on the results, the final feeding mass ratios of drugs were used to prepare the triple-drug-loaded porous microparticles. However, because OME could not be released from the enteric nanoparticles in the stomach, we measured the released amounts of MTZ and OME from the MTZ/OME-loaded porous

microparticles in the SIF (pH 6.8).

The drug loadings of the triple-drug-loaded porous microparticles were not detected because the quantitative analysis of the three drugs together is difficult. However, the entrapment efficiencies of the drugs were maintained at approximately 100% by emulsion electrospray, which indicates the absence of a competitive relationship among the drugs. The maximum MTZ concentration in the preparation of the MTZ/AMO-loaded porous microparticles was selected to be 3.5 mg/mL because the solubility of MTZ in dichloromethane is limited. Similarly, the maximum feeding amount of AMO was 40 mg due to the limited solubility of AMO in water. The drug loading would be higher if a higher amount of drug is dissolved in the spray solution. If the entrapment efficiency of three drugs and the polymer concentration were set to 100 % and 1 %, respectively, the loading capacity of AMO, MTZ, and OME would be 22.88 %, 9.80 %, and 0.85 %, respectively.

Due to the problem of simultaneous quantitative determination of three drugs, the release profiles of three drugs from the triple-drug loaded porous microparticles were not investigated in the present study. But the release profiles of drugs from dual-drug loaded porous microparticles with different drug loading have been studied, and the results indicated that there were no competition relationship among the drugs. Therefore, the AMO, MTZ and OME enteric nanoparticles can be sustainly release from the triple-drug loaded porous gastroretentive microparticles in the stomach, and the OME would immediately release from the nanoparticles when the enteric nanoparticles transported to the duodenum. The triple-drug loaded porous

microparticles could supply a better therapeutic strategy for *H. pylori* infection due to synergistic effect of three drugs.

The dose influences the *in vitro* inhibition effect of porous microparticles and free drugs on *H. pylori*; in particular, an excessive dose of antibiotics would completely clear *H. pylori* within a short time. Conversely, the antibacterial activities of the free drugs and triple-drug-loaded porous microparticles would not be obvious if the drug doses are too low. AMO plays a key role in the anti-*H. pylori* effect of the triple therapy, and the concentration of AMO in the free drugs and the triple-drug-loaded porous microparticles was 0.125 mg/L (MIC_{50} = 0.125 mg/L). The other drugs were also added at the decided mass ratios.

In addition, the *in vivo* elimination of drugs also influences the concentration of drugs, and we simulated the *in vivo* elimination of drugs during the *in vitro H. pylori* growth inhibition study. The elimination half-times of MTZ, AMO, and OME are different, and we referred to the elimination half-time of AMO (approximately 2 h, i.e., the drug concentrations would be reduced by half every 2 h) [29, 30] in this study because AMO plays a key role in the anti-*H. pylori* activity. *H. pylori* treated with the free drugs began to grow after 1 h, whereas *H. pylori* was continuously reduced in the presence of the porous microparticles because of the sustained drug release.

Conclusions

Several novel multiple-drug delivery systems have been developed as combination therapies and have become increasingly popular in clinical practice. The dose ratio of drugs is a key factor for multiple-drug administration because it will

influence the treatment outcome and cause side effects. In the present study, we prepared triple-drug-loaded porous microparticles by emulsion electrospray for combination therapy for the treatment of *H. pylori* infection. More importantly, we focused on studying the dose ratio of the drugs in this multiple-drug delivery system, and the mass ratios of the released drugs were ensured to be in accordance with the dose ratios in the recommend regimen by changing the drug loadings. We first prepared two different dual-drug-loaded porous microparticles (MTZ/OME and MTZ/AMO) to optimize the feeding mass ratios of MTZ to OME and MTZ to AMO and then prepared the triple-drug-loaded porous microparticles according to the decided mass ratios of drugs. The triple-drug-loaded porous microparticles can be retained in the stomach for more than 8 h. The *in vivo H. pylori* clearance studies showed that the triple-drug-loaded porous microparticles exhibit a more complete *H. pylori* clearance effect than the free drugs. The results indicate that the adjustment of the drug loadings is an effective approach for controlling the released amounts of drugs by diffusion-dependent multiple drug delivery systems, and the triple-drug-loaded porous microparticles have the potential to be used in clinical practice for the treatment of *H. pylori* infection.

Acknowledgements

We are grateful to Prof. Zou Quanming for the *H. pylori* strain 26695 and SPF C57BL/6 mice supply (Department of Clinical Microbiology and Clinical Immunology, Third Military Medical University, Chongqing of China) and Dr. Huang Haiping (Department of Pathology, Chongqing Cancer Hospital, Chongqing of China)

for the help of histopathological analysis. The authors acknowledge the financial assistance provided by National Basic Research Program of China (973 Program, Grant No. 2014CB541603) and National Natural Science Foundation of China (Grant No.31200713).

References

1. J. Jingou, H. Shilei, L. Weiqi, W. Danjun, W. Tengfei and X. Yi, *Colloids Surf B*, 2011, **83**, 103-107.
2. S. C. Sundararaj, M. V. Thomas, T. D. Dziubla and D. A. Puleo, *Acta biomaterialia*, 2014, 115-125.
3. L. Zhang, J. Xia, Q. Zhao, L. Liu and Z. Zhang, *Small*, 2010, **6**, 537-544.
4. H.-C. Shin, A. W. G. Alani, D. A. Rao, N. C. Rockich and G. S. Kwon, *J Controlled Release*, 2009, **140**, 294-300.
5. T. P. Richardson, M. C. Peters, A. B. Ennett and D. J. Mooney, *Nat Biotechnol*, 2001, **19**, 1029-1034.
6. T. A. Holland, Y. Tabata and A. G. Mikos, *J Controlled Release*, 2005, **101**, 111-125.
7. T. Liu, G. Wu, Y. Zheng, D. Wismeijer, V. Everts and Y. Liu, *Clin Oral Implan Res*, 2013, 1-10.
8. J. Ji, S. Hao, D. Wu, R. Huang and Y. Xu, *Carbohyd Polym*, 2011, **85**, 803-808.
9. Z. Hussain, H. Katas, M. C. I. Mohd Amin, E. Kumolosasi, F. Buang and S. Sahudin, *Int J Pharm*, 2013, **444**, 109-119.
10. A. K. Jain and S. K. Jain, *J Drug Target*, 2013, 1-11.
11. B. Jeong, Y. H. Bae and S. W. Kim, *J Controlled Release*, 2000, **63**, 155-163.
12. Y. Wang, Y. Zhang, B. Wang, Y. Cao, Q. Yu and T. Yin, *J Nanopart Res*, 2013, **15**, 1-12.
13. C. Chen, L. Zhou, J. Geng, J. Ren and X. Qu, *Small*, 2013, **9**, 2793-2800.
14. H. Wang, Y. Zhao, Y. Wu, Y.-l. Hu, K. Nan, G. Nie and H. Chen, *Biomaterials*, 2011, **32**, 8281-8290.
15. H. Nie, Y. Fu and C.-H. Wang, *Biomaterials*, 2010, **31**, 8732-8740.
16. A. Harris, *Brit Med Bull*, 1998, **54**, 195-205.
17. J. Misiewicz, A. Harris, K. Bardhan, S. Levi, C. O'Morain, B. Cooper, G. Kerr, M. Dixon, H. Langworthy and D. Piper, *Gut*, 1997, **41**, 735-739.
18. D. Y. Graham and L. Fischbach, *Gut*, 2010, **59**, 1143-1153.
19. R. A. Ishak, G. A. Awad, N. D. Mortada and S. A. Nour, *J Controlled Release*, 2007, **119**, 207-214.
20. R. Umamaheshwari, S. Ramteke and N. K. Jain, *AAPS PharmSciTech*, 2004, **5**, 60-68.
21. D. Vaira, L. Gatta, C. Ricci, L. D'Anna and M. Miglioli, *Digest Liver Dis*, 2001, **33**, 788-794.
22. S. Hao, Y. Wang, B. Wang, Q. Zou, H. Zeng, X. Chen, X. Liu, J. Liu and S. Yu, *Int J Pharm*, 2014, **463**, 10-21.
23. P. Bardonnet, V. Faivre, W. Pugh, J. Piffaretti and F. Falson, *J Controlled Release*, 2006, **111**, 1-18.
24. P. Reed and B. Johnston, *Biomed Pharmacother*, 1997, **51**, 13-21.

25. S. Hao, Y. Wang, B. Wang, J. Deng, X. Liu and J. Liu, *Mat Sci Eng C-Mater*, 2013, **33**, 4562-4567.
26. R. P. Aquino, G. Auriemma, T. Mencherini, P. Russo, A. Porta, R. Adami, S. Liparoti, G. D. Porta, E. Reverchon and P. Del Gaudio, *Int J Pharm*, 2013, **440**.
27. A. Streubel, J. Siepmann and R. Bodmeier, *Eur J Pharm Sci*, 2003, **18**, 37-45.
28. Y. Shen, J. Chen, Q. Liu, C. Feng, X. Gao, L. Wang, Q. Zhang and X. Jiang, *Int J Pharm*, 2011, **413**, 184-193.
29. G. Houghton, P. Thorne, J. Smith, R. Templeton and J. Collier, *Brit J Clin Pharmaco*, 1979, **8**, 337-341.
30. E. H. TURGUT and M. ÖZYAZICI, *FABAD J. Pharm. Sci*, 2004, **29**, 39-49.

Table 1 Effect of different feeding amounts of MTZ on the characteristics of the MTZ/OME-loaded porous microparticles (mean ± SD, n = 3) [a].

Feeding amount of MTZ	MTZ (%)		OME (%)	
(mg)	LC [b]	EE [c]	LC	EE
20	15.92±1.20	100.31±3.10	2.06±0.14	100.00±3.96
25	19.20±1.92	100.62±4.11	2.00±0.88	100.97±3.09
30	22.13±2.30	100.31±2.86	1.89±0.14	99.00±4.11
35	24.59±2.58	99.05±3.12	1.86±0.29	101.05±3.22

[a] The feeding amount of OME nanoparticles was 6.0 mg

[b] LC: Loading capacity

[c] EE: Entrapment efficiency

Table 2 Effect of different feeding amounts of AMO on the characteristics of the MTZ/AMO-loaded porous microparticles (mean ± SD, n = 3)[a].

Feeding amount of AMO	MTZ (%)		AMO (%)	
(mg)	LC	EE	LC	EE
25	10.72 ± 1.24	100.06 ± 3.49	17.79 ± 2.19	99.64 ± 4.11
30	10.48 ± 1.79	101.33 ± 3.39	20.66 ± 2.19	99.84 ± 3.30
35	10.03 ± 2.85	100.31 ± 3.40	23.31 ± 2.18	99.91 ± 3.20
40	9.59 ± 2.84	99.14 ± 3.09	25.77 ± 2.11	99.85 ± 3.10

[a] The feeding amount of MTZ nanoparticles was 15 mg

Table 3 Effect of different polymer concentrations on the characteristics of the triple-drug-loaded porous microparticles (mean ± SD, n = 3).

ERS concentration	Size		Zeta potential (mV)		Density (g/cm^3)		Viscosity
(%)	μm	PDI	SGF	Water	Bulk	Tap	(mPa·s)

1%	2.83 ± 0.01	0.201 ± 0.019	41.09 ± 2.44	13.39 ± 2.19	0.025 ± 0.010	0.040 ± 0.007	9.13 ± 0.35
2%	4.90 ± 0.02	0.251 ± 0.028	45.25 ± 2.38	14.78 ± 2.10	0.037 ± 0.007	0.061 ± 0.012	10.26 ± 0.23
3%	8.41 ± 0.02	0.209 ± 0.039	49.08 ± 2.19	16.44 ± 2.19	0.049 ± 0.011	0.090 ± 0.004	11.96 ± 0.16
4%	9.30 ± 0.01	0.147 ± 0.020	52.34 ± 2.91	21.92 ± 2.07	0.054± 0.004	0.110 ± 0.009	14.20 ± 0.13

Figure caption

Fig. 1 The schematic illustration of formation of triple-drug-loaded porous microparticles

Fig. 2 *In vitro* release profiles of MTZ (A -a) and OME (A-b) from the MTZ/OME-loaded porous microparticles with different feeding amounts of MTZ in SGF (mg) and release profiles of MTZ (A-c) and OME (A-d) in SIF. Cumulative released amounts of MTZ and OME from the MTZ/OME-loaded porous microparticles with the following different feeding amounts of MTZ in SIF: 20 mg (B-a), 25 mg (B-b), 30 mg (B-c), and 35 mg (B-d).

Fig.3 *In vitro* release profiles of AMO (A-a) and MTZ (A-b) from the MTZ/AMO-loaded porous microparticles with different feeding amounts of AMO in SGF (mg). Cumulative released amounts of MTZ and AMO from the MTZ/AMO-loaded porous microparticles with the following different feeding amounts of AMO in SGF: 25 mg (B-a), 30 mg (B-b), 35 mg (B-c), and 40 mg (B-d).

Fig. 4 (A) SEM and TEM images of the triple-drug-loaded porous microparticles with different ERS concentrations. (B) SEM images of triple-drug-loaded porous microparticles after incubation in SGF for different times.

Fig. 5 (A) FTIR spectra of drugs, polymers, EL 100-55 nanoparticles, and drug-loaded porous microparticles. (B) XRD patterns of drugs, polymers, EL 100-55 nanoparticles, drug-loaded porous microparticles, and physical mixture of drugs and polymers.

Fig. 6 (A) Cell viability after treatment with different concentrations of the triple-drug-loaded porous microparticles (4% ERS) for 24 h. (B) Cell viability after treatment with blank microparticles and the triple-drug-loaded porous microparticles (50 mg/L) with different ERS

concentrations for different times. (**$P \leq 0.01$ and *$P \leq 0.05$ compared with the control group)

Fig. 7 Gamma scintigraphic images of ^{131}I-labeled triple-drug-loaded porous microparticles in rabbit. (The outline of the rabbit was drawn manually based on the actual rabbit).

Fig. 8 SPECT, CT and SPECT/CT fused images of ^{131}I-labeled triple-drug-loaded porous microparticles 8 h after their oral administration in rabbit with transverse (A), sagittal (B), and coronal (C) views. (D) Radioactive counts of the ^{131}I-labeled porous microparticles in the ROI every two minutes.

Fig. 9 (A) Sustained antibacterial effect of free drugs, blank porous microparticles, and triple-drug-loaded porous microparticles. The values are the means ± S.D. (n = 3). Colonization of H. pylori in the stomach after the oral administration of free drugs and triple-drug-loaded porous microparticles with a low dose (B), middle dose, (C) and high dose (D). (**$p < 0.01$ and *$p < 0.05$ compared with control group; QD: once daily; BID: twice daily)

Fig. 10 Histopathological findings in the gastric mucosa of C57BL/6 mice 1 month after H. pylori inoculation and triple therapy with the low, middle, and high doses of the free drugs (QD and BID dosing) and triple-drug-loaded porous microparticles (QD dosing). The tissues were stained with hematoxylin/eosin. (QD: once daily; BID: twice daily. Blue arrows: inflammatory cell infiltration; Black arrows: superficial damage and atrophic changes; Red arrows: necrosis of the epithelium)

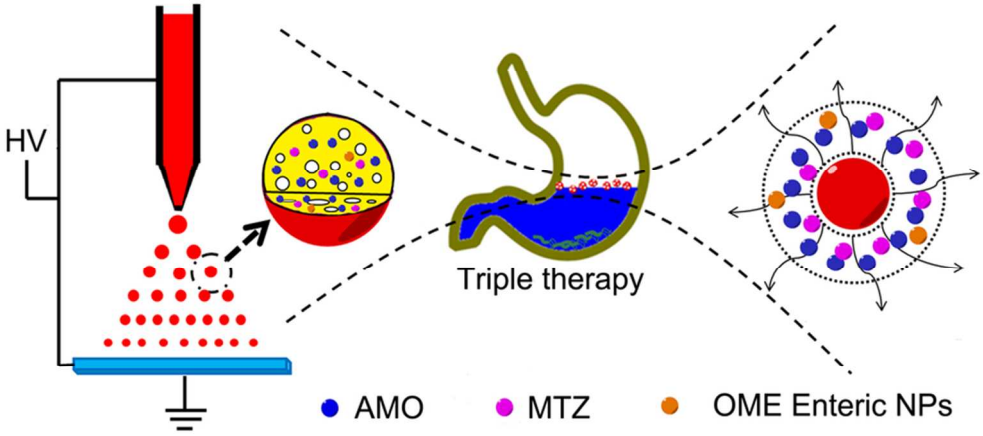

The triple-drug loaded porous gastroretentive microparticles were prepared to treat Helicobacter Pylori infection, and the mass ratios of released drugs were in accordance with that in triple therapy regimen.
39x19mm (600 x 600 DPI)

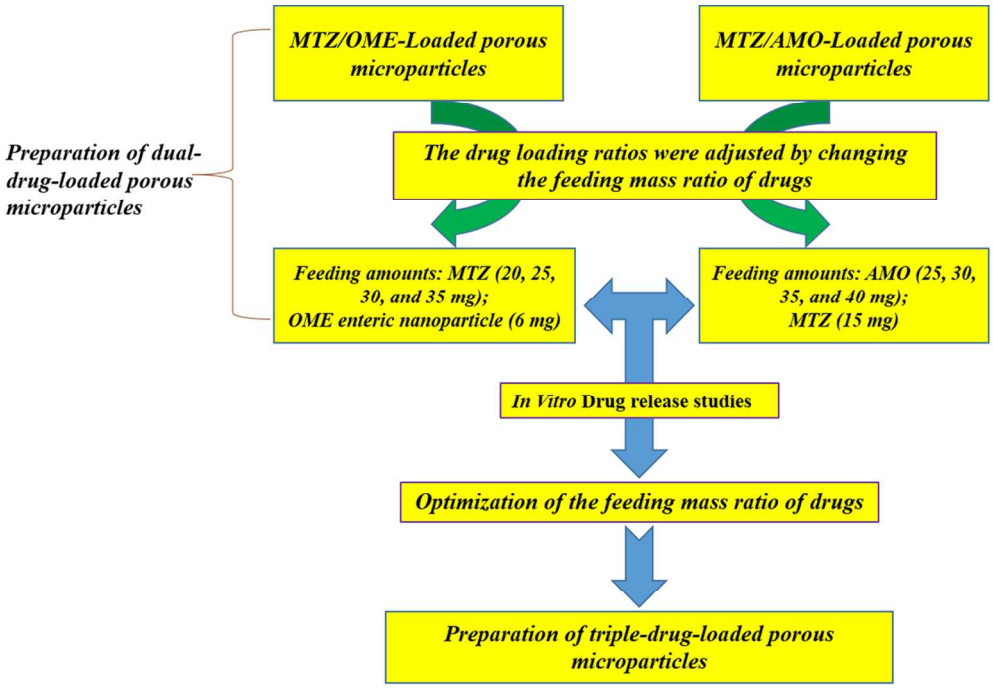

The schematic illustration of formation of triple-drug-loaded porous microparticles
116x79mm (300 x 300 DPI)

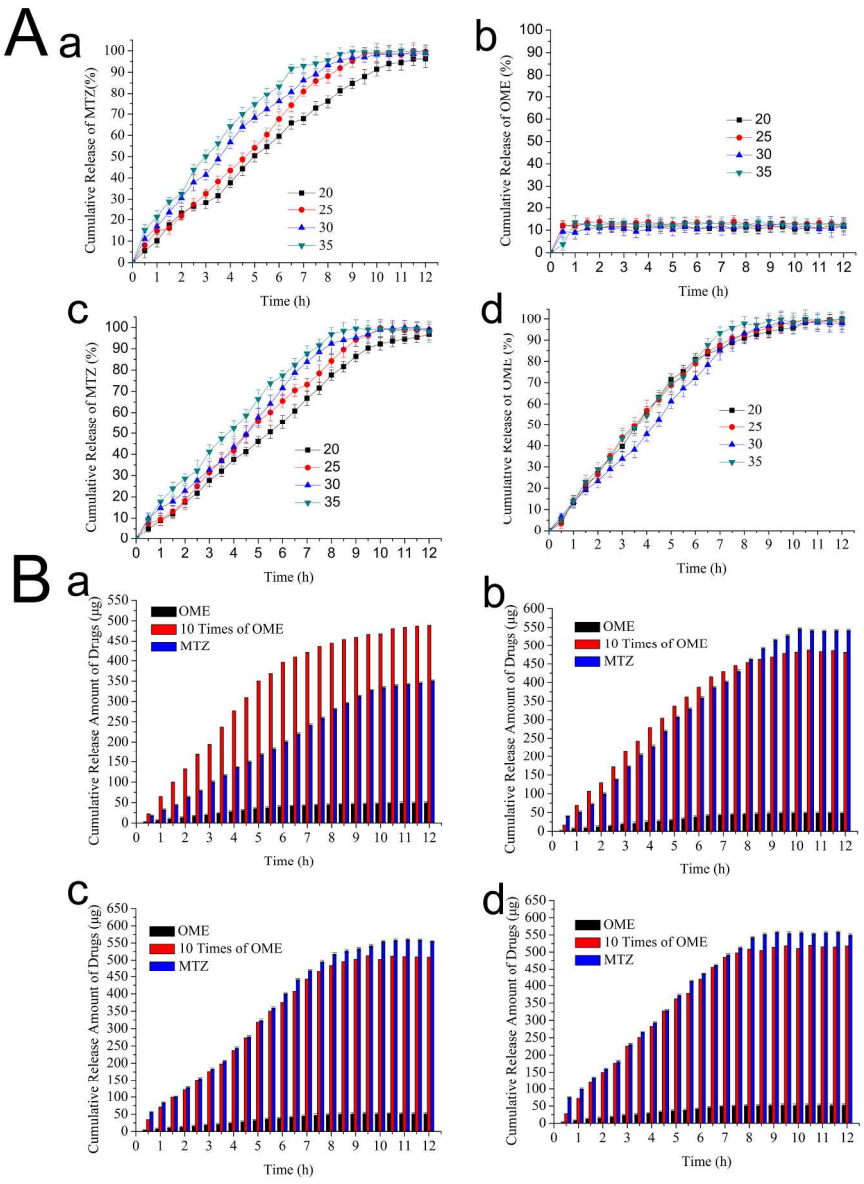

In vitro release profiles of MTZ (A -a) and OME (A-b) from the MTZ/OME-loaded porous microparticles with different feeding amounts of MTZ in SGF (mg) and release profiles of MTZ (A-c) and OME (A-d) in SIF. Cumulative released amounts of MTZ and OME from the MTZ/OME-loaded porous microparticles with the following different feeding amounts of MTZ in SIF: 20 mg (B-a), 25 mg (B-b), 30 mg (B-c), and 35 mg (B-d).
226x299mm (300 x 300 DPI)

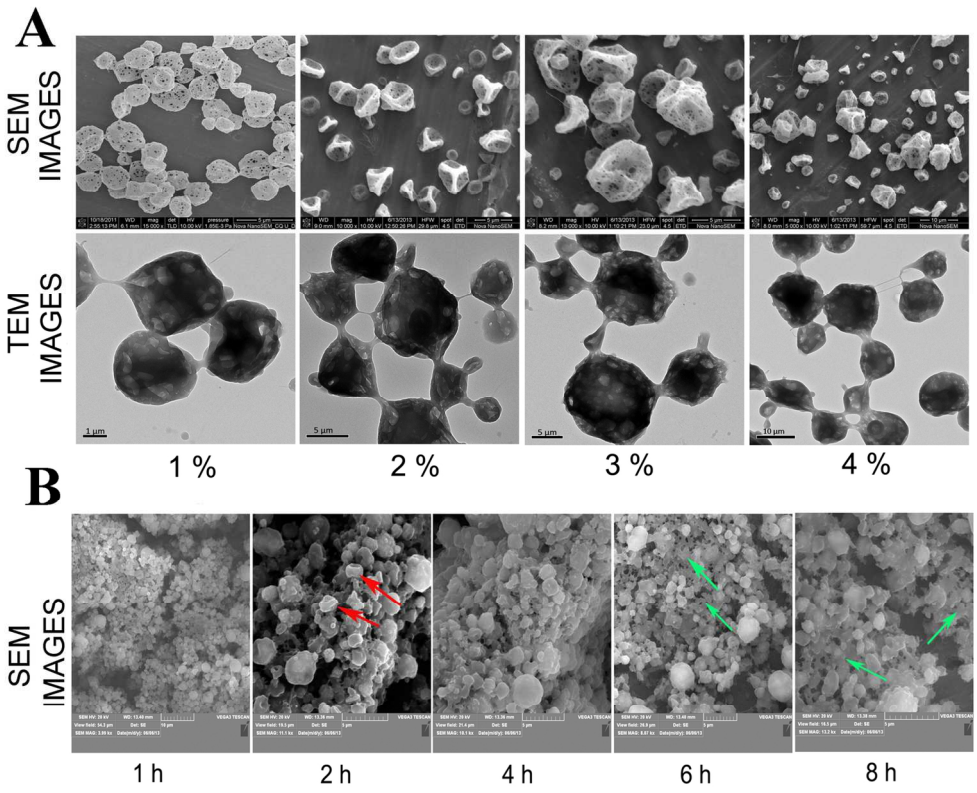

(A) SEM and TEM images of the triple-drug-loaded porous microparticles with different ERS concentrations. (B) SEM images of triple-drug-loaded porous microparticles after incubation in SGF for different times.
140x115mm (300 x 300 DPI)

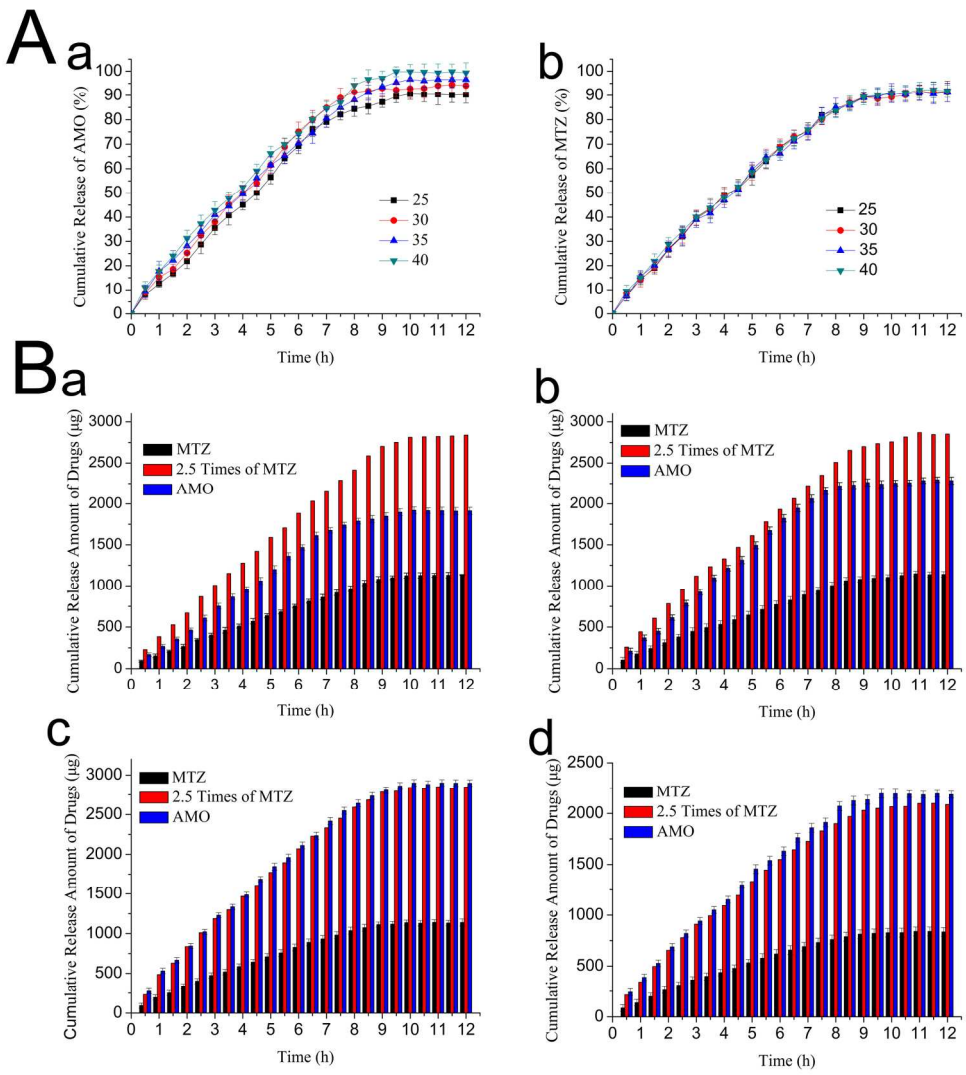

In vitro release profiles of AMO (A-a) and MTZ (A-b) from the MTZ/AMO-loaded porous microparticles with different feeding amounts of AMO in SGF (mg). Cumulative released amounts of MTZ and AMO from the MTZ/AMO-loaded porous microparticles with the following different feeding amounts of AMO in SGF: 25 mg (B-a), 30 mg (B-b), 35 mg (B-c), and 40 mg (B-d).
186x202mm (300 x 300 DPI)

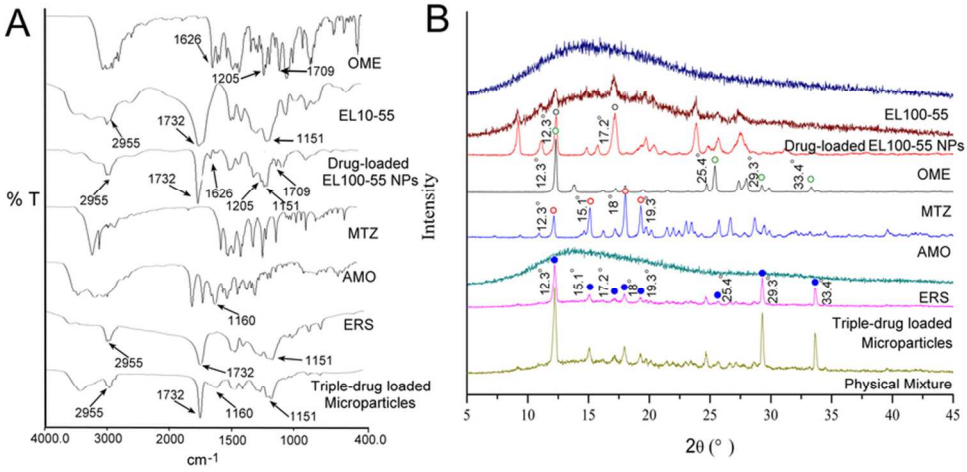

(A) FTIR spectra of drugs, polymers, EL 100-55 nanoparticles, and drug-loaded porous microparticles. (B) XRD patterns of drugs, polymers, EL 100-55 nanoparticles, drug-loaded porous microparticles, and physical mixture of drugs and polymers.
81x40mm (300 x 300 DPI)

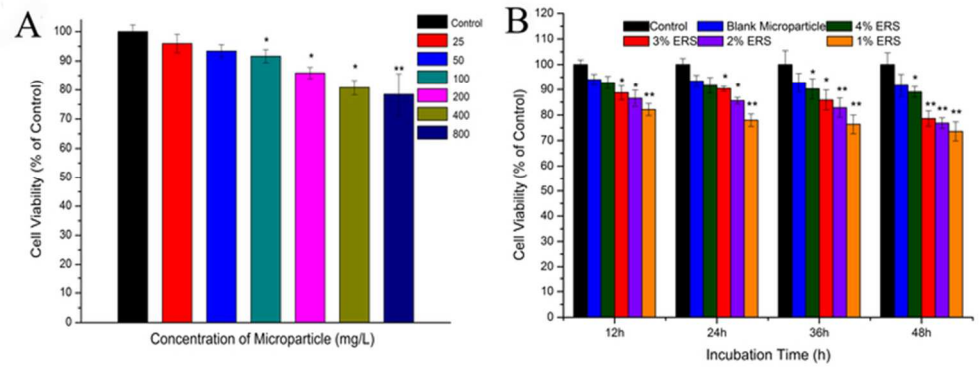

(A) Cell viability after treatment with different concentrations of the triple-drug-loaded porous microparticles (4% ERS) for 24 h. (B) Cell viability after treatment with blank microparticles and the triple-drug-loaded porous microparticles (50 mg/L) with different ERS concentrations for different times. (**P ≤ 0.01 and *P ≤ 0.05 compared with the control group)
64x24mm (300 x 300 DPI)

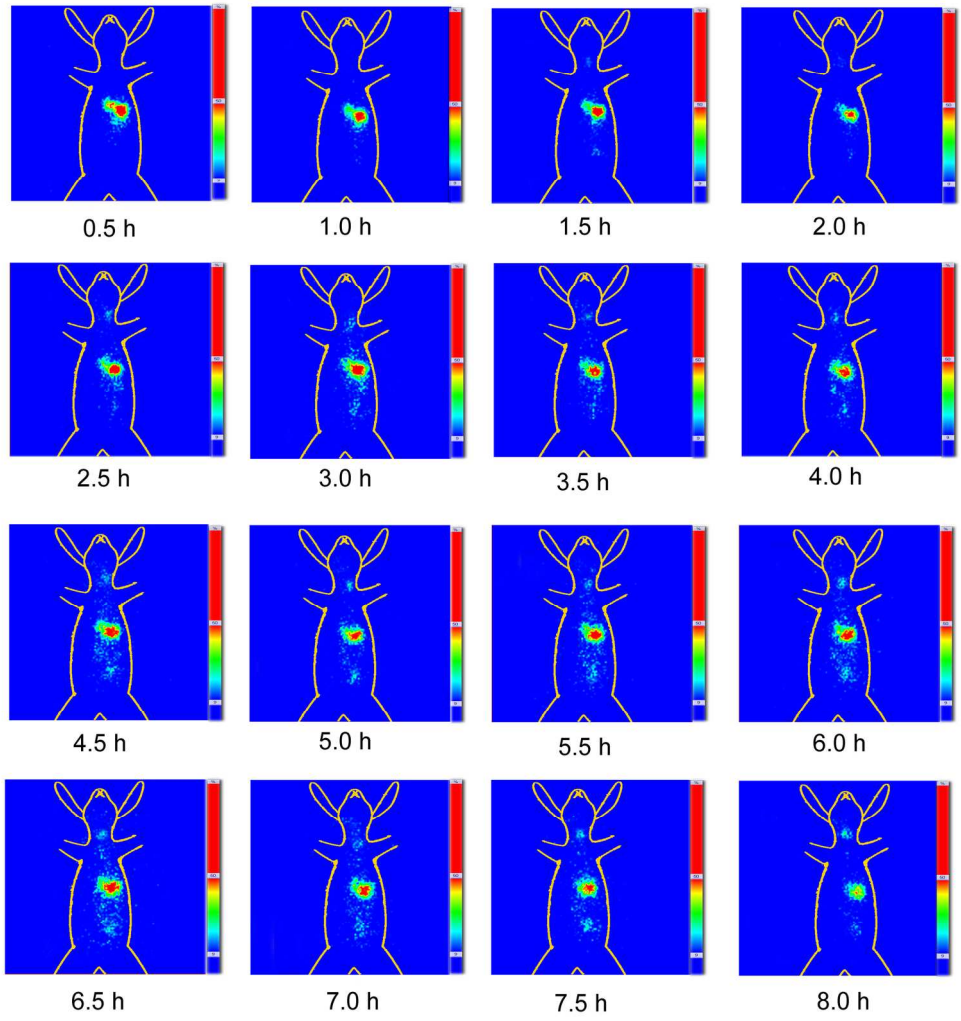

Gamma scintigraphic images of 131I-labeled triple-drug-loaded porous microparticles in rabbit. (The outline of the rabbit was drawn manually based on the actual rabbit).
171x182mm (300 x 300 DPI)

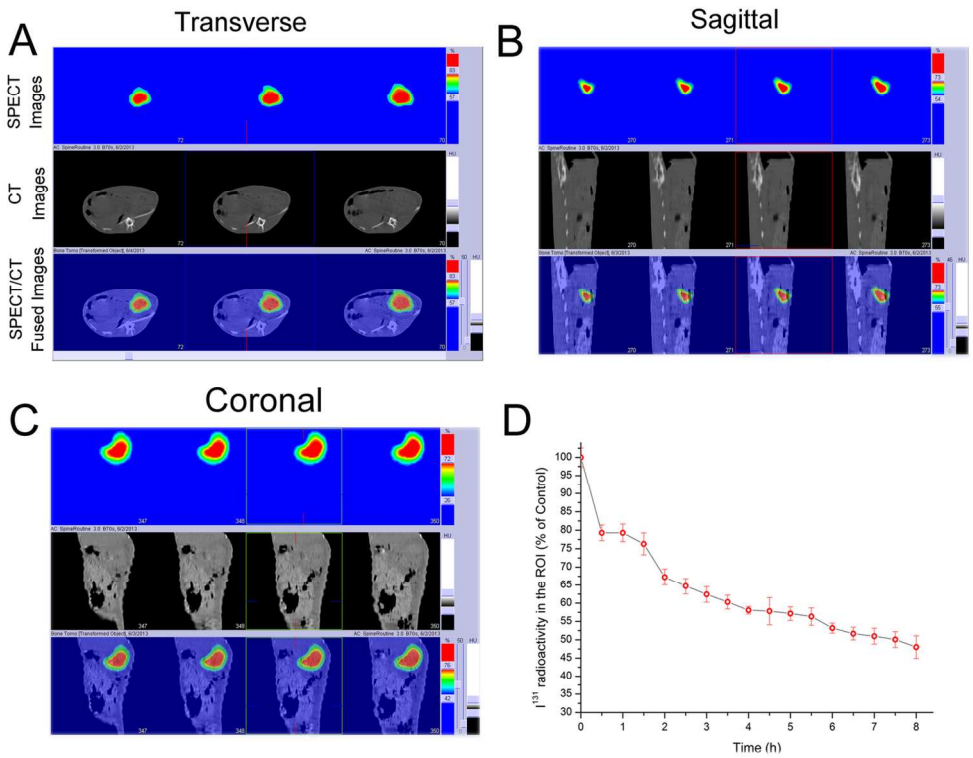

SPECT, CT and SPECT/CT fused images of 131I-labeled triple-drug-loaded porous microparticles 8 h after their oral administration in rabbit with transverse (A), sagittal (B), and coronal (C) views. (D) Radioactive counts of the 131I-labeled porous microparticles in the ROI every two minutes.
133x104mm (300 x 300 DPI)

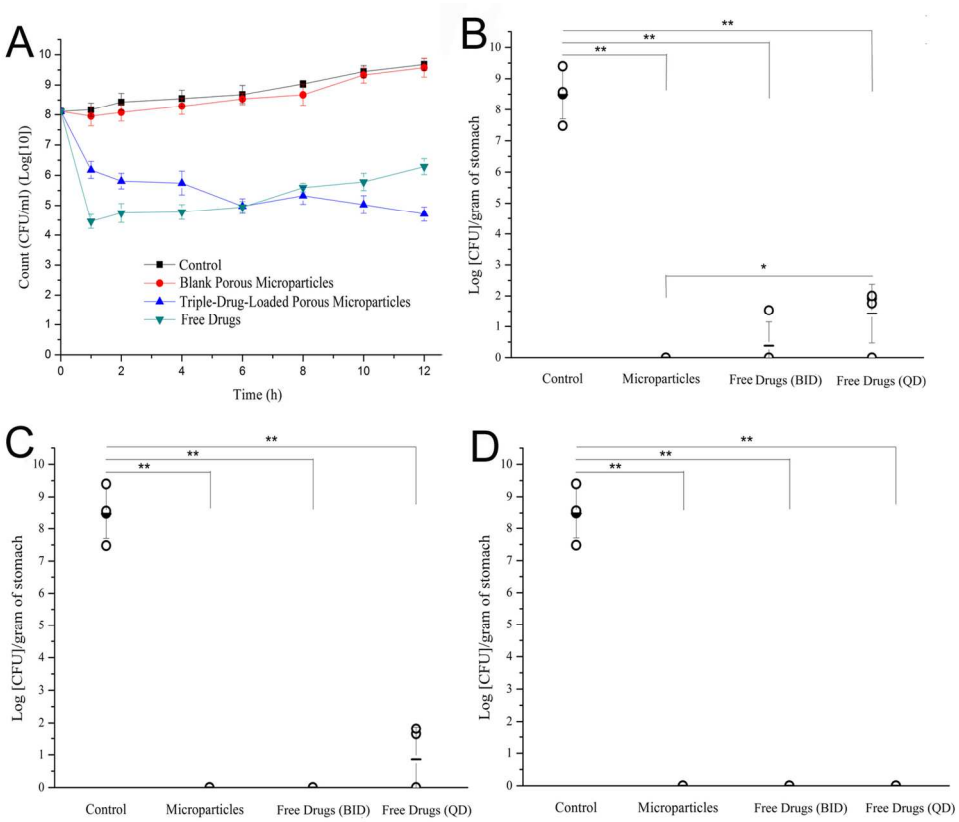

(A) Sustained antibacterial effect of free drugs, blank porous microparticles, and triple-drug-loaded porous microparticles. The values are the means ± S.D. (n = 3). Colonization of H. pylori in the stomach after the oral administration of free drugs and triple-drug-loaded porous microparticles with a low dose (B), middle dose, (C) and high dose (D). (**p < 0.01 and *p < 0.05 compared with control group; QD: once daily; BID: twice daily)
68x57mm (600 x 600 DPI)

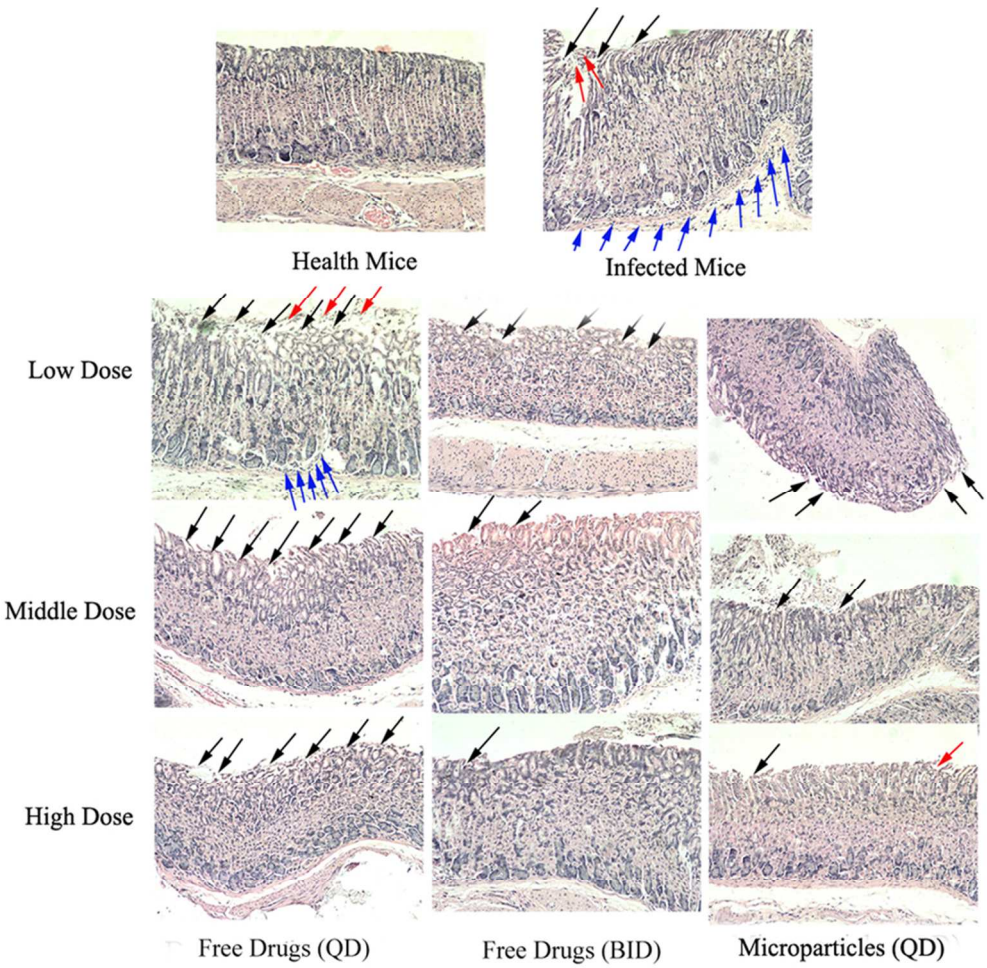

Histopathological findings in the gastric mucosa of C57BL/6 mice 1 month after H. pylori inoculation and triple therapy with the low, middle, and high doses of the free drugs (QD and BID dosing) and triple-drug-loaded porous microparticles (QD dosing). The tissues were stained with hematoxylin/eosin. (QD: once daily; BID: twice daily. Blue arrows: inflammatory cell infiltration; Black arrows: superficial damage and atrophic changes; Red arrows: necrosis of the epithelium)
80x77mm (300 x 300 DPI)